SPECIAL PROJECT PROGRESS REPORT

All the following mandatory information needs to be provided. The length should *reflect the complexity and duration* of the project.

Reporting year	2025 (2nd year of the project)
Project Title:	Simulation of extremes of Arctic sea ice reduction with a rare event algorithm in EC-Earth3
Computer Project Account:	……spberago……
Principal Investigator(s):	Francesco Ragone
Affiliation:	Royal Meteorological Institute of Belgium (RMI)
Name of ECMWF scientist(s) collaborating to the project (if applicable)	……. ……
Start date of the project:	01 January 2024
Expected end date:	31 December 2026

Computer resources allocated/used for the current year and the previous one

		Previous year		Current year	
		Allocated	Used	Allocated	Used
High Performance Computing Facility	(units)	32,000,000	31,963,528	14,000,000	9,903,590
Data storage capacity	(Gbytes)	90,000	50,000	125,000	100,000

Summary of project objectives (10 lines max)

In this project, we apply the Giardina-Kurchan-Lecomte-Tailleur (GKLT) rare event algorithm [1-7] to ensemble simulations with EC-Earth3 [8] to increase the sampling efficiency of extreme Arctic sea ice lows. Taking advantage of the improved statistics provided by the algorithm, we estimate the probabilities of extreme sea ice lows and we investigate their physical drivers. The aim is to better understand the relative importance of winter-spring sea ice-ocean preconditioning vs. spring-summer thermodynamic and dynamic processes in favouring extremely low sea ice conditions. Finally, we are interested in the probability of ultra-rare but high impact events, including sea ice area anomalies larger in magnitude than observed in 2012 and events with a total disappearance of Arctic sea ice for one year under current climate conditions.

Summary of problems encountered (10 lines max)

As reported in 2024, the computational resources required by the simulations with the rare event algorithm are larger than the original estimates based on experience with other models. In the previous report, we identified the likely sources of the issue: 1) rebuilding of NEMO restart files; 2) too large output frequency of IFS; 3) inefficient tar-compression of output files; 4) redundant rearrangement of model code. We addressed the first and the fourth issue, but overall we did not manage to substantially decrease the computational costs. We therefore refocused the project on experiments of Type 3 and 4. Compared to experiments of Type 1 and 2, these are more relevant for real world applications such as seasonal climate predictions, and are also more appropriate to investigate physical drivers of low sea ice states on sub-seasonal scale, in particular to disentangle the relative contribution of weather variability *vs.* winter sea ice-ocean preconditioning.

Summary of plans for the continuation of the project (10 lines max)

Using EC-Earth3, we finalized a 250-year stationary control run, one control ensemble and two rare event algorithm ensemble simulations. These ensembles are initialized from a neutral winter sea ice initial condition (Exp. Types 3-4; N=300). We estimated the probability of sea ice lows larger in magnitude than observed in 2012. We are currently preparing a sea ice area, volume and surface energy budget analysis to quantify the relative contributions of sea ice dynamics vs. thermodynamic processes to low sea ice states [6,9]. To quantify the relative contributions of winter sea ice preconditioning *vs.* weather variability to extreme sea ice lows, we will use "anomaly initialization" [10] to start another pair of control and rare event ensemble simulation from a state with reduced sea ice thickness compared to the first three ensembles. A "long memory" experiment to investigate the statistics of the extremes after two years of rare event simulation is planned for 2026.

List of publications/reports from the project with complete references

We published a rare event algorithm study with the intermediate complexity coupled climate model PlaSim-LSG. This study provided us with the necessary expertise to reasonably apply the algorithm to the comprehensive climate model EC-Earth3:

Sauer J., F. Massonnet, G. Zappa, and F. Ragone, 2025: Ensemble design for seasonal climate predictions: studying extreme Arctic sea ice lows with a rare event algorithm. Earth System Dynamics, **16(3)**, 683-702, https://doi.org/10.5194/esd-16-683-2025.

Summary of results

1. Setting-up EC-Earth3 on "Atos" and publication of PlaSim-LSG rare event algorithm study

We partly dedicated the first six project months to technical aspects of setting-up and working with EC-Earth version 3.3.1 (IFS-36r4-T255L91, NEMO3.6-ORCA1L75) [8] on the High-Performance Computing Facility "Atos". We produced a 250-year post-spin up control run under fixed year-2000 greenhouse gas conditions (Figure 1) and we implemented the rare event algorithm into the EC-Earth environment. We tested to what extent the statistical properties of the simulated climate depend on whether the model is restarted from "IFS-restart files" vs. perturbed and unperturbed "IFS-initial condition files". We found that the "IFS-initial condition files" can be used to implement small random perturbations required for the simulations with the algorithm. Regarding the basic climate state in the model, the simulated pan-Arctic sea ice area and annual mean sea ice thickness are representative of the observed 1979-2015 mean Arctic sea ice climatology (cf. Figure 1, Supplementary Information of [6] and page 207 of [11]).

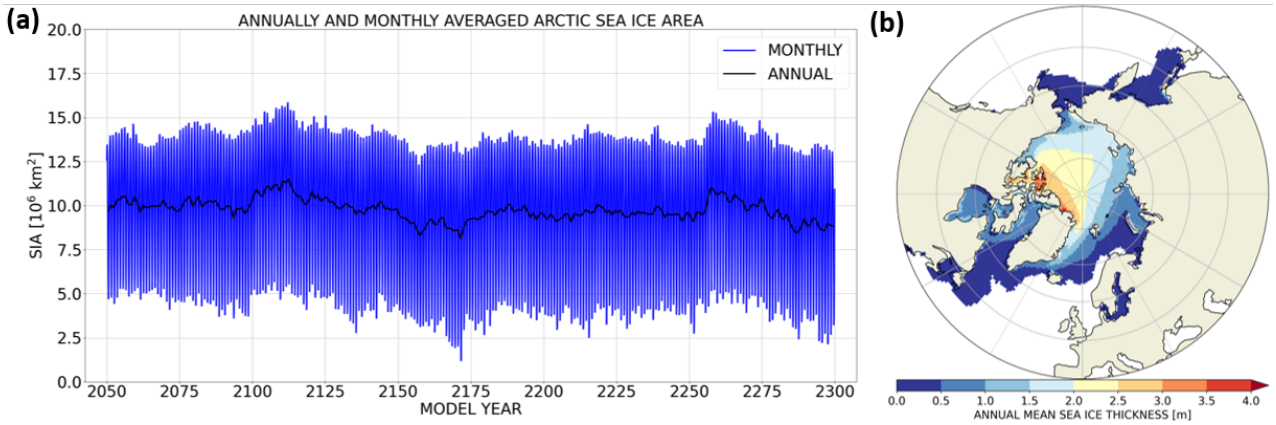

Figure 1: Control run with EC-Earth version 3.3.1: (a) Pan-Arctic sea ice area and (b) annual mean sea ice thickness computed as an average over the model years 2050-2299.

In parallel and as a preparation of the experiments with EC-Earth3, we performed a set of rare event algorithm and control ensemble simulations with the intermediate complexity coupled climate model PlaSim-LSG [12-13]. These ensembles started from slightly perturbed identical initial conditions sampled from a control run. Such an ensemble design corresponds to the set-up used for the experiments "Type 3" and "Type 4" with EC-Earth3. The work with PlaSim-LSG resulted in our first publication within this special project [7]. In [7], we demonstrated the applicability of using the algorithm to improve the sampling efficiency of extremes of pan-Arctic sea ice area reduction within one single melting season. Using a computational cost of order 10^3 years, we simulated sea ice lows with probabilities of less than 10^{-5} and with amplitudes larger than observed in 2012. By comparing the statistics of summer sea ice area between four ensembles initialized from four different winter states, we quantified the relative contributions of winter sea ice-ocean preconditioning *vs.* (sub)seasonal weather variability to extreme sea ice lows. We investigated thermodynamic states of the atmosphere-sea ice-ocean system leading to sea ice lows with probabilities of less than 10^{-5}.

The rare event algorithm involves a killing-cloning procedure where trajectories leading to extremely negative sea ice area anomalies form replicas at the expense of trajectories leading to less negative sea ice area anomalies [3-7]. The strength and frequency of this trajectory resampling is determined by parameter values. While a reasonable order of magnitude of those parameter values can be derived from the characteristic time scales of the dynamics (standard deviation and decorrelation time), the optimal choice of the parameter values remains empirical [3-7]. The small computational cost of PlaSim-LSG compared to EC-Earth3 allowed us to systematically investigate the sensitivity of the sampling of the extremes as a function of different parameter values. This step therefore substantially contributed to the expertise required to find an appropriate set-up of the rare event simulations with the comprehensive climate model EC-Earth3 within this special project.

2. Experimental design of rare event simulations with EC-Earth3

We perform three groups of control and rare event algorithm ensemble simulations with $N = 300$ trajectories (table 1). In the first group, the ensembles are initialized from a neutral winter sea ice initial condition sampled from the EC-Earth3 control run (the initial condition is taken from model year 2237). These ensembles are initialized on 01 March and run until 01 October (Figure 2(a)). The initial condition is selected according to the neutrality of February-March mean anomalies in the pan-Arctic sea ice area and in the cumulative area with sea ice thickness equal or larger than 1.80 metres (SIT1.80). Consistent with [14], an analysis of the control run showed that the late winter cumulative area with sea ice thickness equal or larger than a given threshold, in particular SIT1.80, is more relevant in determining the risk of an extremely negative late summer sea ice area anomaly than the pan-Arctic sea ice volume and the sea ice area itself.

The first group of experiments is completed and consists of a control ensemble without the rare event algorithm and two rare event simulations (Figures 2(a), 3 and 4). One rare event simulation is performed with the pan-Arctic sea ice area as an observable, i.e., the experiment is designed to directly improve the sampling efficiency of trajectories leading to low states of sea ice area (Figures 3(a,b) and 4(a); referred to as "SIA experiment" or "OBSERVABLE: SIA" hereafter). The other rare event simulation is performed with the pan-Arctic sea ice volume as an observable, i.e., the experiment is designed to improve the sampling efficiency of trajectories leading to low states of sea ice volume (Figures 3(c,d) and 4(b); referred to as "SIV experiment" or "OBSERVABLE: SIV" hereafter). As discussed in section 3 in "Summary of the results", the SIV experiment improves the sampling of low states in the pan-Arctic sea ice area in an indirect way.

Table 1:N=300 trajectory control and rare event algorithm ensembles. The first group is initialized with a neutral sea ice initial condition taken from 01 March 2237 of the 250-year control run. They are run from 01 March to 01 October and are finalized. The two low winter sea ice ice initial condition experiments (group 2) will be conducted in 2025 based both on the computational resources available through this special project and through the ones from the regular budget of the Royal Meteorological Institute (RMI) in Belgium. Both the the special project and RMI resources will be used for the "Long memory" experiments (group 3) in year 2026.

Experiment group	Characteristics	Timing of conduction	# SBUs
1) Neutral winter sea ice initial condition	Control ensemble	10/2024	4,000,000
	Rare event simulation with sea ice area as observable	11/2024	13,000,000
	Rare event simulation with sea ice volume as observable	12/2024 – 01/2025	13,000,000
2) Low winter sea ice initial condition	Control ensemble	07/2025	4,000,000
	Rare event simulation with sea ice volume as observable	08/2025	13,000,000
3) Long memory: running "1)" for another 12 months	12 months control ensemble	01/2026–04/2026	6,850,000
	7 months with the algorithm	01/2026–04/2026	13,000,000

For the second group of experiments, we will use "anomaly initialization" [10] to add to the initial condition of the first group on a grid point level the sea ice thickness and sea ice concentration difference between 2012 and the 2000-2011 climatology. We derive those anomalies from a NEMO4.2.2 historical sea ice-ocean reanalysis available in our laboratory. From a technical point of view, we verified that EC-Earth3 can be initialized and run from that modified initial condition without any problems. This second group will include a control ensemble without the rare event algorithm and a rare event simulation with the sea ice volume as an observable, both running from 01 March to 01 October. The experiments of "group 2" will be performed in 2025. "Group 2" requires about 17,000,000 SBUS and will both be based on the computational resources of this special project and on the resources from the regular budget of the Royal Meteorological Institute (RMI) in Belgium.

In 2026, we will use the special project and RMI resources to run the experiments of "group 3". These will consist in a 12 months continuation of the SIV experiment of "group 1". While the model months October to February will be run without the algorithm, the period between the subsequent March to September will be run without and with the algorithm respectively.

The combination of the three groups of experiment allows us to quantify the relative contribution of winter sea ice preconditioning *vs.* sub-seasonal and seasonal weather variability to the risk and amplitudes of extreme Arctic sea ice lows. The required accuracy in the representation of late summer sea ice area variability is given in the EC-Earth set-up used in this project (Figure 2(a-c)). Thus, the standard deviations of August-September mean sea ice area and of the difference between August-September and late winter sea ice area in the EC-Earth3 control ensemble are $0.4 \bullet 10^6$ km^2 respectively (Figure 2(a)). For these two metrics, the standard deviations of the observed residuals relative to a linear trend fitted to the period 1979-2024 in European Organisation for the Exploitation of Meteorological Satellites (EUMETSAT) Ocean and Sea Ice Satellite Application Facility (OSI SAF) data [15] are 0.38 10^6 km^2 and 0.42 10^6 km^2 respectively (Figure 2(b,c)).

3. Importance sampling of extreme Arctic sea ice lows with EC-Earth3

Throughout the melting season, trajectories generated with the sea ice area experiment show a systematic shift towards lower sea ice area values compared to the control ensemble (Figure 3(a)). This corresponds to the importance sampling of trajectories leading to extremely negative sea ice area anomalies on average over the entire simulation period. Compared to the full simulation period, the shift reaches its largest amplitude in late summer, and the distribution of August-September mean sea ice area values obtained with the algorithm includes values below the minimum in the control ensemble (Figure 3(b)). While the control ensemble delivers two (zero) trajectories with an August-September mean sea ice area anomaly equal or smaller than -2.5 (-3) control ensemble standard deviations, the algorithm provides 20 extremes with sea ice area values at least 2.5 control ensemble standard deviations below the control ensemble mean. Due to the trajectory resampling, not all extremes obtained with the rare event sampling are independent (see [3-7] for more details). However, the sea ice area experiment still provides seven different initial ancestors on March 1st that lead to August-September mean sea ice area values of at least 2.5 control ensemble standard deviations below the control ensemble mean. Consequently, one can find 7 extremes in the ensemble fully independent with respect to the perturbation set at the initialization on March 1st, yielding improved statistics on the extremes compared to the control ensemble.

The sea ice volume experiment is designed to perform importance sampling of trajectories leading to extremely negative sea ice volume anomalies on average over the entire simulation period. However, the result in Figure 3(c,d) demonstrates that this also allows to increase the sampling of low states of the late summer sea ice area. The sea ice volume experiment is efficient in sampling low states of late summer sea ice area as it directly improves the sampling of trajectories developing an anomalously strong sea ice thinning during spring. As shown in [7,14], anomalously low spring sea ice thickness states act as a preconditioning for anomalously low states in late summer sea ice area. The sea ice volume experiment delivers 48 (30) trajectories leading to an August-September mean sea ice area value of 2.5 (3) standard deviations below the control ensemble mean. 5 (1) events are fully independent with respect to the perturbation set at initialization.

As described in [7], the ensembles can be used to compute the probabilities of observing an August-September mean sea ice area value equal or smaller than a certain threshold (Figure 4). The control and rare event algorithm estimates are consistent with each other where they overlap. The algorithm, however, allows to estimates probabilities below the ones available from the control (below 10^{-4} and 10^{-3} for the sea ice volume and area experiment respectively for a computational cost of order 10^2). This can for example be used to provide an estimate of the probability to observe a sea ice area anomaly larger in magnitude than the observed 2012 sea ice area anomaly relative to a forced signal (for example relative to a linear trend fitted to the period 1979-2024; Figure 2(b)). The probability of a fluctuation with larger amplitudes than the deviation of the 2012 sea ice area from the 1979-2024 linear trend estimated with these two experiments is in the order of 10^{-3} (cf. Figures 2(b) and 4)).

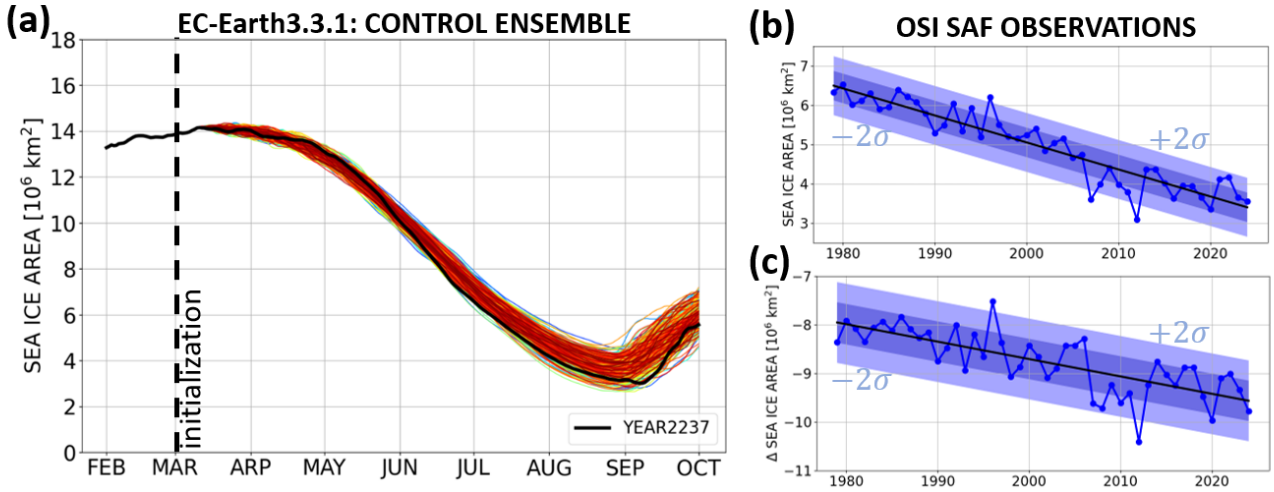

Figure 2: (a) Pan-Arctic sea ice area in the neutral winter sea ice initial condition control ensemble with N=300 trajectories. (b-c) European Organisation for the Exploitation of Meteorological Satellites (EUMETSAT) Ocean and Sea Ice Satellite Application Facility (OSI SAF) data [15]. (b) August-September mean pan-Arctic sea ice area and (c) the difference between August-September and February-March mean sea ice area (i.e. the reduction of sea ice area from the annual maximum to the annual minimum).

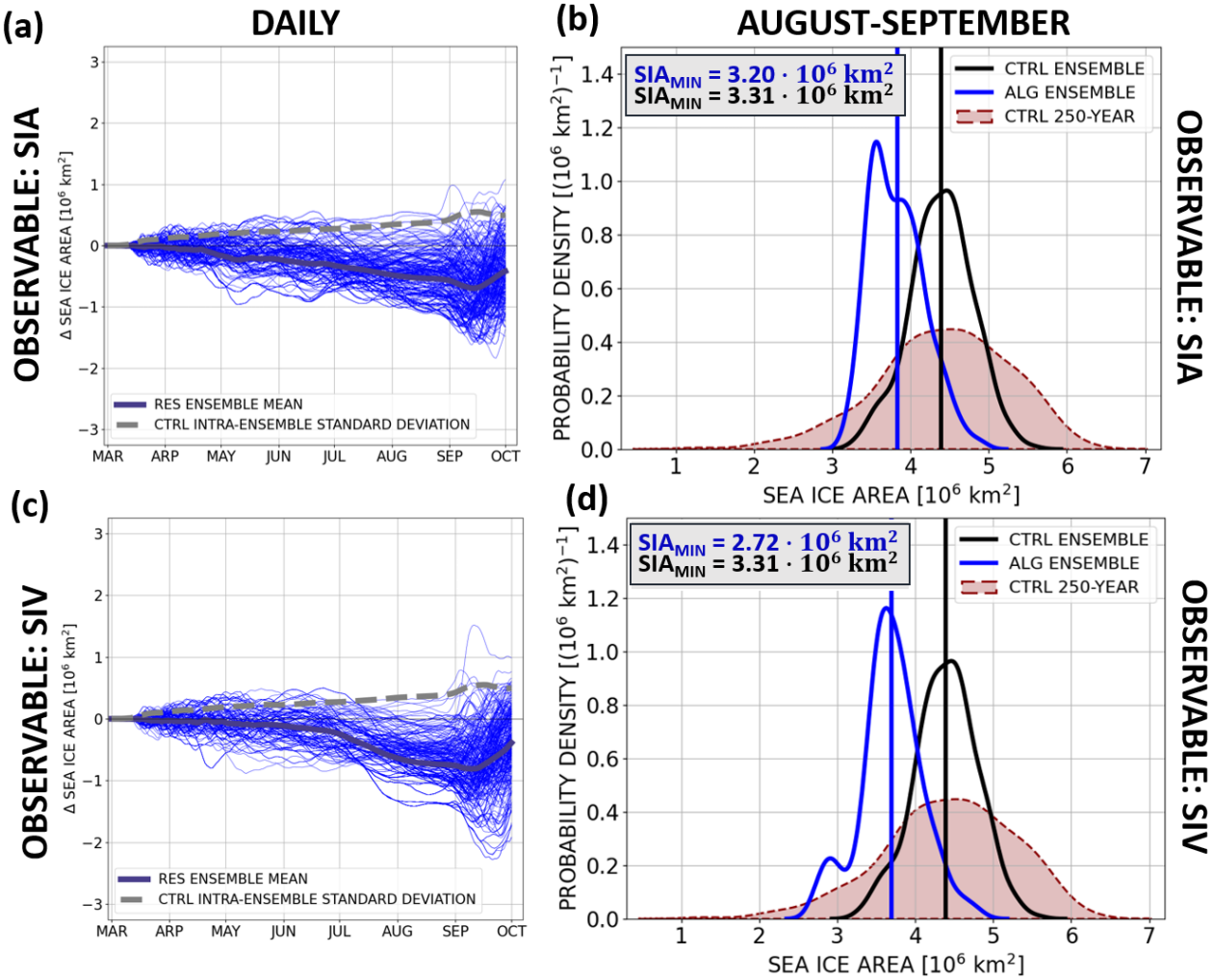

Figure 3:EC-Earth3: Pairs of N=300 trajectory control and rare event algorithm ensemble simulations initialized from a neutral winter sea ice state sampled from the control run (model year 2237 in Figure 1(a)). Panels (a,b) show the sea ice area (SIA) and (c,d) the sea ice volume (SIV) experiment. (a,c) Trajectories (thin blue lines) and ensemble mean (thick blue lines) of daily pan-Arctic sea ice area anomalies [10⁶ km²] obtained with the rare event algorithm and computed relative to the climatology of the control ensemble. The gray dashed line in (a,c) shows the intra-ensemble standard deviation in the control ensemble. (b,d) August-September mean pan-Arctic sea ice area: Probability density functions for (black) the control ensemble, (blue) the two rare event algorithm ensembles and (red) the full 250-year control run. The vertical lines show the means of the distributions.

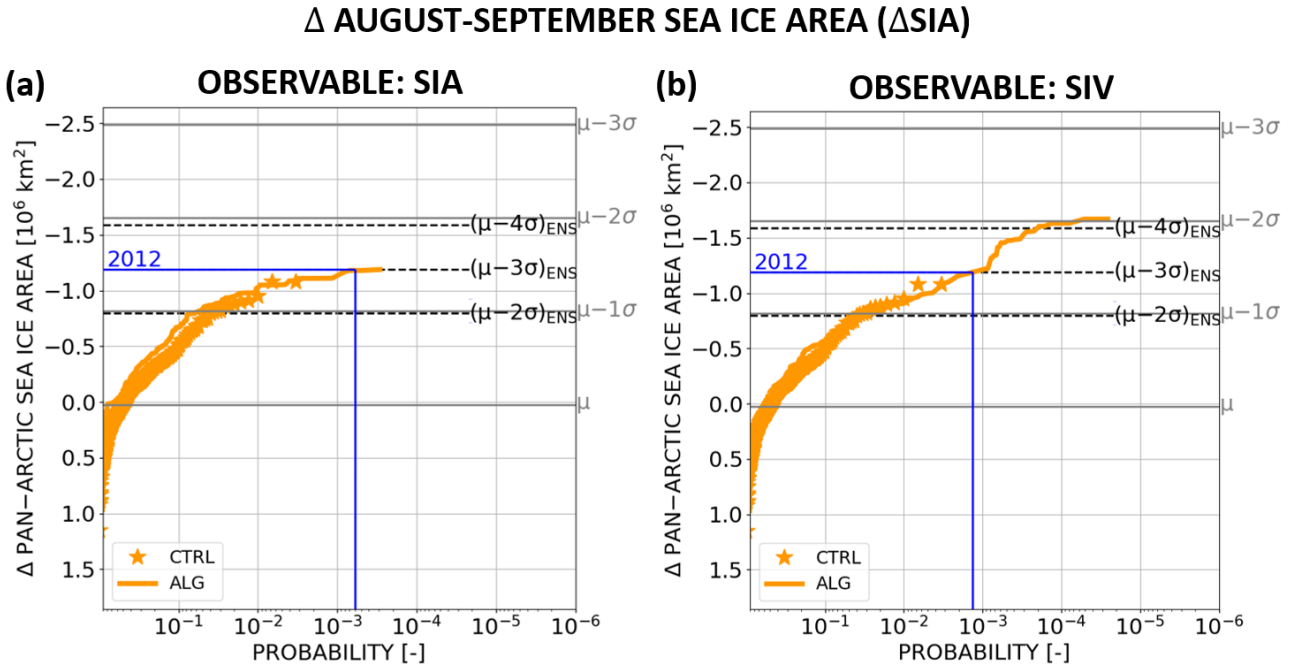

Figure 4: EC-Earth3 neutral sea ice initial condition ensembles: Probabilities (x-axes) of AS mean pan-Arctic sea ice area anomalies equal to or smaller than a given threshold (y-axes) and computed relative to the control ensemble mean. Panel (a) shows the SIA and (b) the SIV experiment. The orange stars and solid lines show the control and rare event algorithm estimates. The grey (black) labels on the right indicate how many control run (control ensemble) standard deviations a sea ice area value is below the mean of the 250-year control run (below the control ensemble mean). The blue lines mark the observed 2012 AS mean sea ice area anomaly relative to a linear trend fitted to the period 1979-2024 according to OSI SAF (Figure 2(b); [15]).

4. Physical processes leading to extreme sea ice lows in EC-Earth3

Based on the output of the SIV experiment with the algorithm, we performed first analyses of the physical processes leading to extreme reductions of the pan-Arctic sea ice area within one single melting season (Figures 5-8). We discuss the trajectory leading to the most extremely negative August-September (AS) mean sea ice area anomaly available from this ensemble (referred to as "AS ΔSIA ALG MIN"). We also address the mean physical properties on average over all trajectories characterized by AS mean sea ice area values more than 2.5 standard deviations below the control ensemble mean (such a composite is referred to as "AS $\Delta\text{SIA} \leq -2.5\sigma$" hereafter; see [4,6] for details about the computation of composites with the algorithm). In Figures 5 and 7, we complement this analysis by a second composite which is exactly defined as "AS ΔSIA $\leq -2.5\sigma$", but where we exclude all trajectories that share the same ancestor at the initialization time as the "AS ΔSIA ALG MIN" trajectory (referred to as "AS $\Delta\text{SIA} \leq -2.5\sigma \mid \text{ancestor index} \neq 131$). This allows to verify whether the "AS ΔSIA $\leq -2.5\sigma$" composite reflects the typical behaviour of the extremes in a statistical sense or whether it is simply dominated by the "AS ΔSIA ALG MIN" behaviour.

In August-September, the "AS ΔSIA ALG MIN" trajectory is associated with enhanced sea ice cover eastern of Greenland and strongly reduced sea ice cover within the entire Pacific-Eurasian side of the Arctic (Figure 5(a,b)). Compared to the observed 2012 event, the sea ice cover is less reduced north-eastern of Svalbard, but much more reduced around the north pole (cf. Figure 5(a,b) and [16]). The "AS $\Delta\text{SIA} \leq -2.5\sigma$" and the "AS $\Delta\text{SIA} \leq -2.5\sigma \mid \text{ancestor index} \neq 131$" composites reveal that the dipole with enhanced and reduced sea ice cover around Greenland and on the Pacific-Eurasian side of the Arctic reflects a common behaviour in this neutral initial condition experiment.

Regarding the seasonal evolution, low sea ice trajectories start to develop negative sea ice area anomalies in late spring-early summer and reach the largest sea ice area anomalies in magnitude in August-September (Figure 6(a,d)). During spring and expressed in the units of control ensemble standard deviations, negative sea ice volume anomalies are larger in magnitude than the area anomalies (Figure 6(a,d)). This indicates that enhanced spring sea ice thinning anticipates the formation of enhanced summer open water area similarly to our findings in [7]. Regarding the geographic location, enhanced early summer sea ice thinning occurs in the interior of the sea ice edge on the Pacific side of the Arctic Ocean (Figure 6(b,c,e,f)).

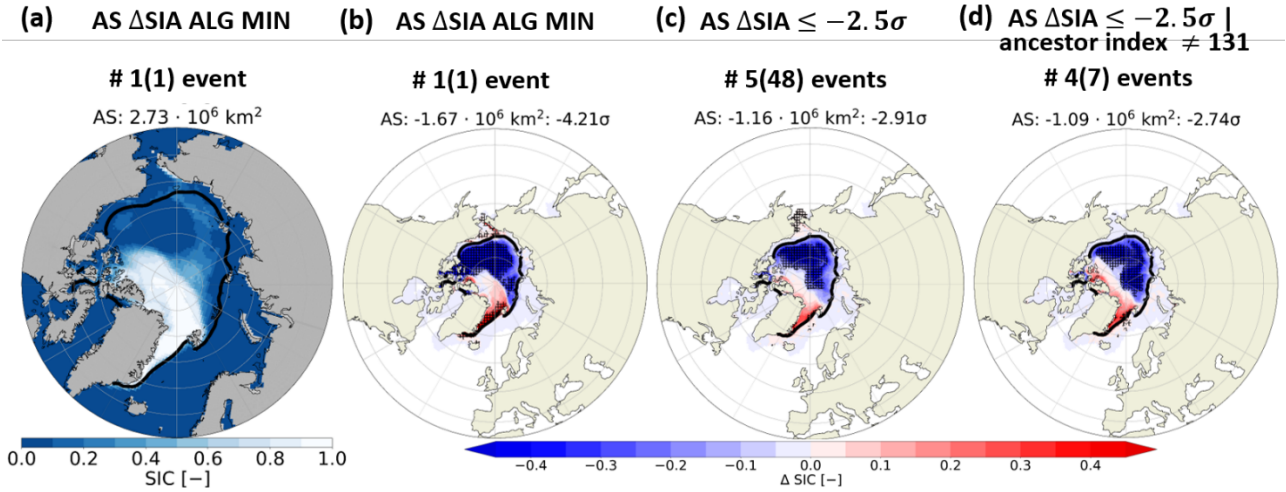

Figure 5: AS mean sea ice concentraion in the SIV experiment with the algorithm in EC-Earth3: (a) Absolute values and (b-d) anomalies relative to the control ensemble mean. Hatching in (b-d) indicates regions where the anomalies are larger in magnitude than the control ensemble standard deviation. Panels (a,b) show the "AS ΔSIA ALG MIN" trajectory and (c,d) the "AS ΔSIA $\leq -2.5\sigma$ *" and "AS ΔSIA* $\leq -2.5\sigma \mid ancestor\,index \neq 131$" *composites. The numbers above the panels indicate the total number of extremes and the number of fully independent events with respect to the random perturbation set during the initialization.*

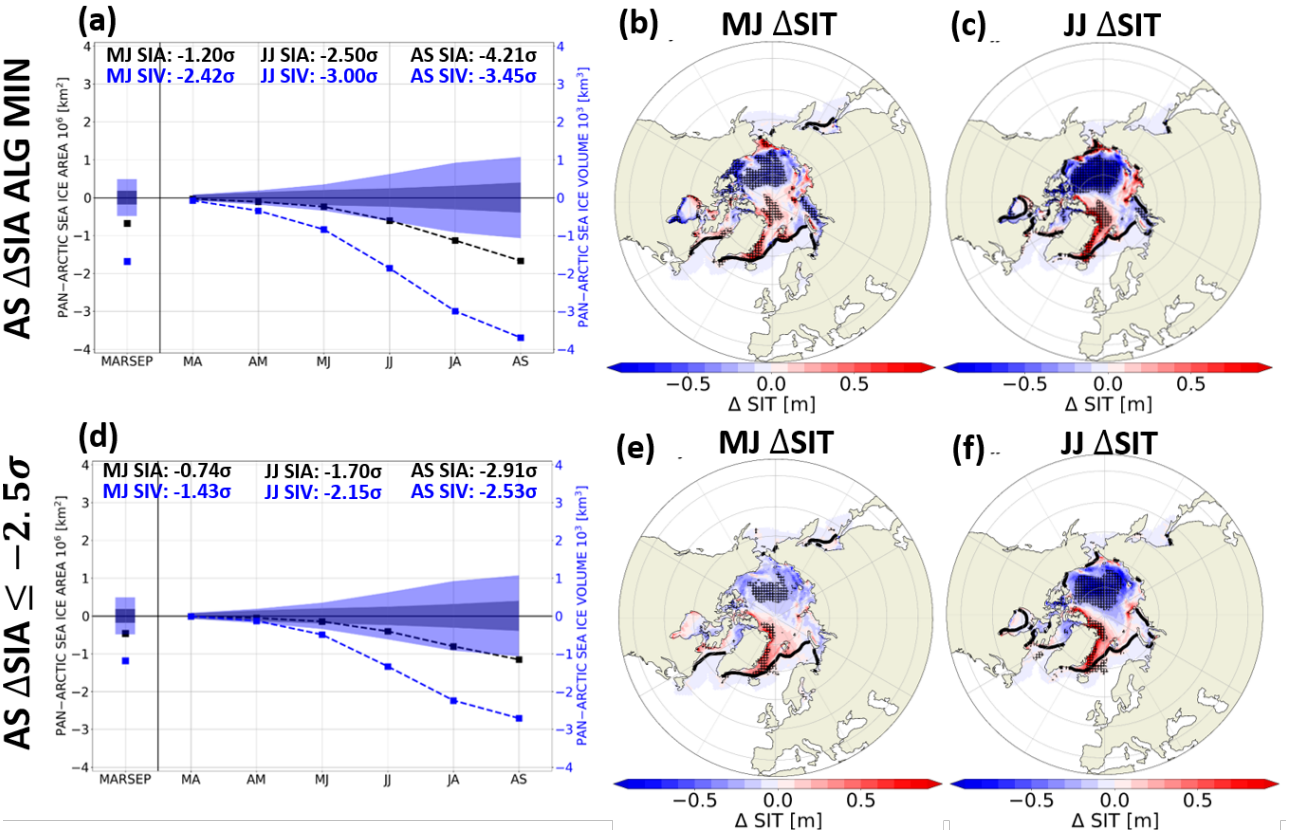

Figure 6: Anomalies relative to the control ensemble mean in the SIV experiment with the algorithm: (a,d) Pan-Arctic sea ice (black) area and (blue) volume and (b,c,e,f) May-June (b,e) and June-July (c,f) sea ice thickness. The shading in (a,d) indicates the control ensemble standard deviation and hatching in (b,c,e,f) indicates regions where the anomalies are larger in magnitude than the control ensemble standard deviation. The solid line in (b,c,e,f) shows the 15% sea ice concentration contour line in the control ensemble mean. Panels (a-c) are based on the trajectory that leads to the lowest AS mean sea ice area values within the experiment and panels (d-f) show a composite over all AS mean sea ice area anomalies equal or smaller than -2.5 control ensemble standard deviations.

The non-uniform spring-summer sea ice thickness anomalies, with negative ones in the central Arctic and positive ones eastern of Greenland, suggests a redistribution of sea ice mass via a dynamic impact of atmospheric circulation anomalies on the sea ice motion. On average, the summer Arctic sea ice motion is characterized by the transpolar drift and an anticyclonic circulation in the Beaufort Gyre underneath anticyclonic mean sea level pressure conditions over the Beaufort Sea (Figure 7(a)).

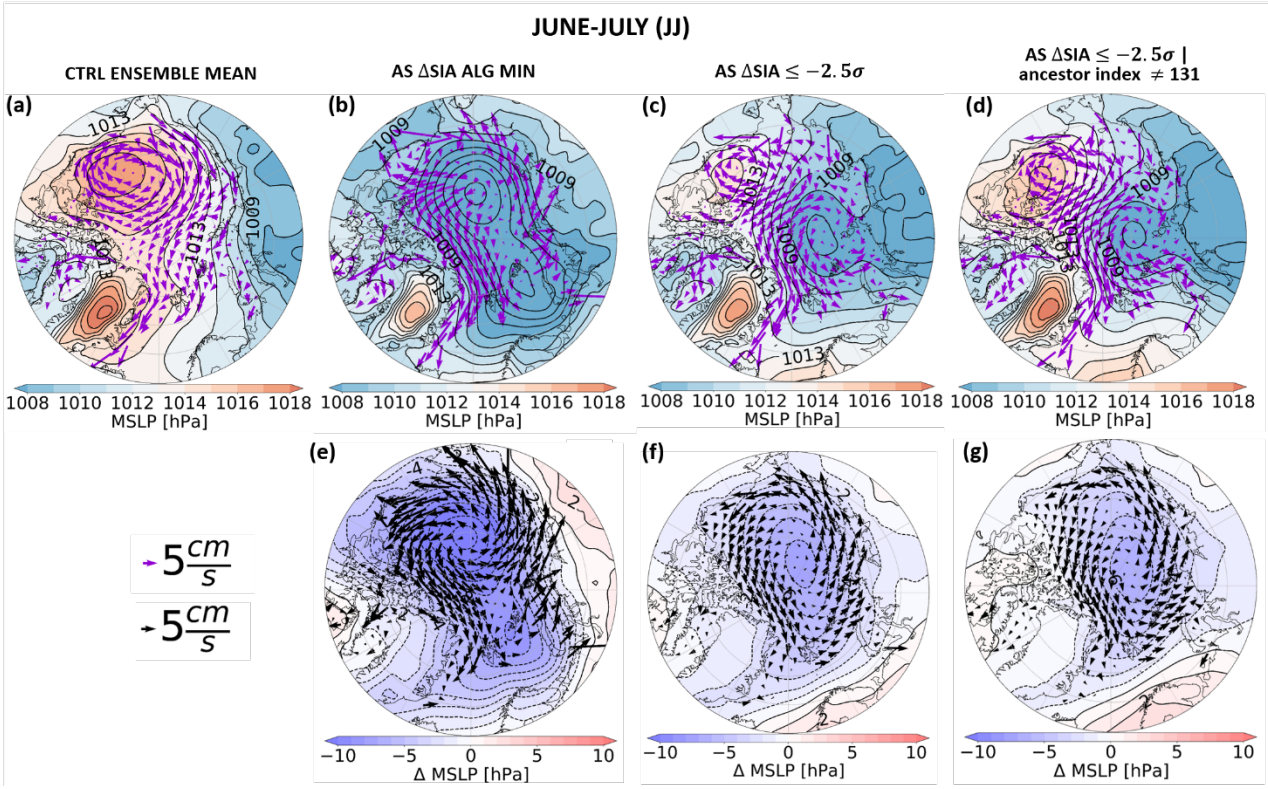

Figure 7: June-July mean mean sea level pressure (1 hPa contour interval) and sea ice motion vectors [cm/s] in the SIV experiment with the algorithm: (a-d) Absolute values and (e-g) anomalies relative to the control ensemble mean. The panel (a) is the control ensemble mean, (b,e) show the "AS ΔSIA ALG MIN" trajectory and (c,f) and (d,g) the AS ΔSIA ≤ −2.5σ | ancestor index ≠ 131 and AS ΔSIA ≤ −2.5σ composites respectively.

In the "AS ΔSIA ALG MIN" trajectory, instead, strongly cyclonic conditions lead to a complete disappearance of the Beaufort Gyre, enhanced sea ice motion out of the central Arctic Ocean towards the American and Eurasian coasts and towards Fram Strait (Figure 7(b,e)). Cyclonic mean sea level pressure and sea ice motion vector anomalies also occur in the "AS ΔSIA $\leq -2.5\sigma$" and the "AS ΔSIA $\leq -2.5\sigma$ | ancestor index $\neq 131$" composites. This reflects that cyclonic anomalies are a typically ingredient of low sea ice states in this experiment (Figure 7(b-g)). A total disappearance of the Beaufort Gyre, however, does not occur systematically on average over multiple extremes (Figure 7(c-d)).

We are currently preparing a sea ice volume budget analysis to quantify the relative contribution of sea ice dynamics to anomalously low sea ice states (Figure 8). In a substantial region on the Pacific side of the North Pole in the "AS ΔSIA ALG MIN" trajectory, the dynamic impact of the large-scale atmospheric circulation on the sea ice motion field explains about 80% of enhanced 01 June-31 July sea ice volume reduction. This is both explained by enhanced sea ice velocity divergence out of the central Arctic Ocean and by advective processes, whereby the former dominates over the latter (Figure 8(b-d)). A substantial contribution of the dynamic impact of atmospheric circulation anomalies on enhanced sea ice volume reduction is also apparent in the "AS ΔSIA $\leq -2.5\sigma$" composite (Figure 8(f-j)).

In the near-future, we will apply a systematic the sea ice volume and area budget analysis to all months of the melting season, computing a spatially integrated budget within the area of climatological mean late summer sea ice cover. This will be complemented by surface energy budget analysis, allowing us to quantify the relative importance of sea ice dynamics vs. thermodynamics to the formation of low sea ice states during the course of the melting season. We will also investigate to what extent the cyclonic anomalies are related to strong synoptic-scale storm or simply reflect persistent negative mean sea ice level pressure anomalies. Finally, the analyses will be extended to the sea ice area experiment.

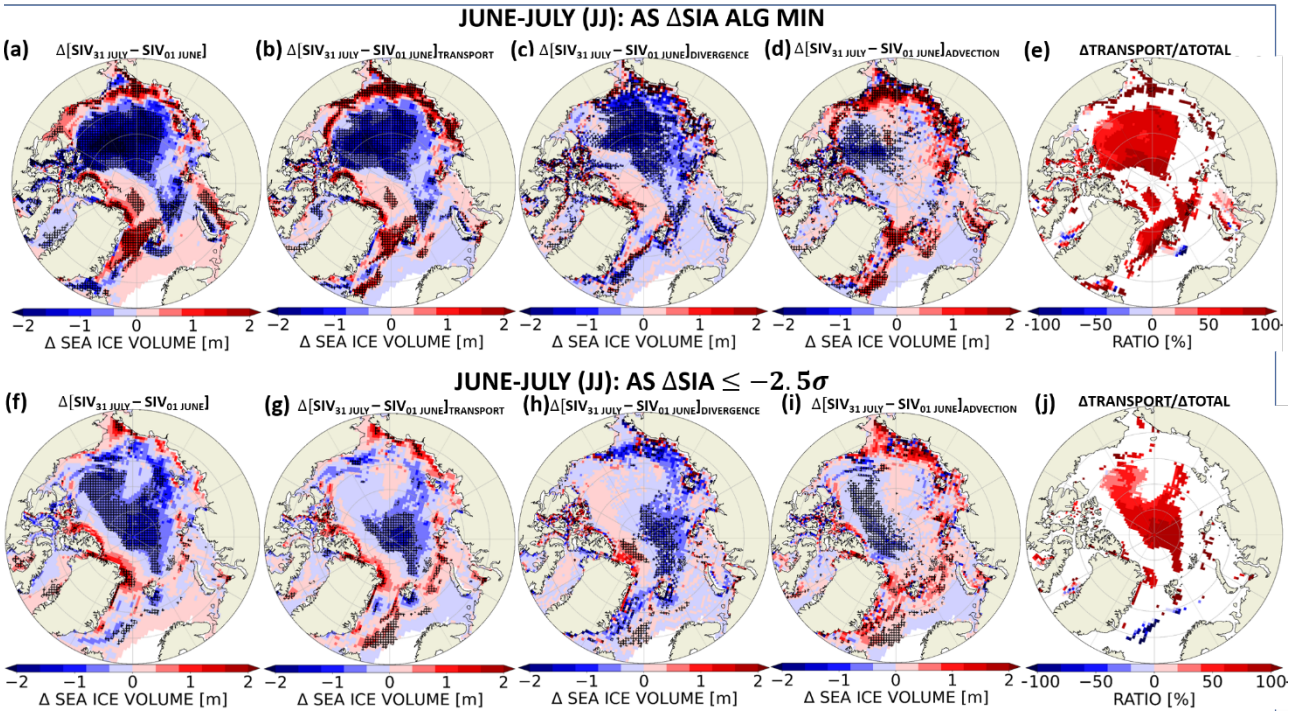

Figure 8: Sea ice volume budget analysis in SIV experiment with the algorithm for the months June-July: Anomalies relative to the control ensemble mean: (a,f) The sea ice volume difference between 01 June and 31 July. (b-d, g-i) as (a,f), but explained by (b,g) the sea ice volume transport (i.e. the sum of advection and divergence),. (c.h) the divergence and (d,i) the advection. (e,j) is the ratio between the transport-driven anomalies of the 01 June to 31 July sea ice volume reduction and the total sea ice volume reduction anomalies. Hatching in (a-d) and (f-i) marks regions where the anomalies are equal or larger in magnitude than the control ensemble standard deviation. The panels (a-e) show the "AS ΔSIA ALG MIN" trajectory and (f-j) the AS ΔSIA $\leq -2.5\sigma$ composites.

References

[1] Del Moral, P. and J. Garnier, 2005: Genealogical particle analysis of rare events, *Ann Appl. Prob.*, **15(4)**, 2496-2534, doi:10.1214/105051605000000566.

[2] Giardina C., J. Kurchan, V. Lecomte, J. Tailleur, 2011: Simulating rare events in dynamical processes, *Journal of Statistical Physics*, **145,** 787-811, doi:10.1007/s10955-011-0350-4.

[3] Ragone, F., J. Wouters and F. Bouchet, 2018: Computation of extreme heat waves in climate models using a large deviation algorithm, *Proc. Natl. Acad. of Sci.*, **115(1)**, 24-29, doi:10.1073/pnas.1712645115.

[4] Ragone, F. and F. Bouchet, 2019: Computation of Extreme Values of Time Averaged Observables in Climate Models with Large Deviation Techniques, *Journal of Statistical Physics*, **179(5)**, 1637-1665, doi:10.1007/s10955-019-02429-7.

[5] Ragone, F. and F. Bouchet, 2021: Rare event algorithm study of extreme warm summers and heatwaves over Europe, *Geophys. Res. Lett.*, **48(12)**, 1-12, doi:10.1029/2020GL091197.

[6] Sauer, J., F. Ragone, F. Massonnet, G. Zappa, J. Demaeyer, 2024: Extremes of summer Arctic sea ice reduction investigated with a rare event algorithm, *Climate Dynamics*, 1-19, doi:10.1007/ s00382-024-07160-y.

[7] Sauer, J., F. Massonnet, G. Zappa, F. Ragone, 2025: Ensemble design for seasonal climate predictions: studying extreme Arctic sea ice lows with a rare event algorithm, *Earth System Dynamics*, **16(3)**, 683-702, doi: 10.5194/esd-16-683-2025.

[8] Döscher, R., M. Acosta, A. Alessandri, P. Anthoni, A. Arneth, T. Arsouze, T. Bergmann, R. Bernadello, S. Bousetta, L. Caron, et al., 2022: The EC-Earth3 Earth System Model for the Climate Model Intercomparison Project 6, *Geoscientific Model Development*, **15(7)**, 2973-3020, doi:10.5194/gmd-2020-446.

[9] Holland, P. R. and R. Kwok, 2011: Wind-driven trends in Antarctic sea-ice drift, *nature geoscience*, 1-8, doi:10.1038/NGEO1627.

[10] Tian, T., S. Yang, M. P. Karami, F. Massonnet, T. Kruschke and T. Koenigk. 2022: Benefits of sea ice initialization for the interannual-to-decadal climate prediction skill in the Arctic in EC-Earth3, *Geosci. Model Dev*, **14**, 4283-4305, doi:10.5194/gmd-14-4283-2021.

[11] Chevallier, M., F. Massonnet, H. Goessling, V. Guémas, and J. Thomas, 2019: The Role of Sea Ice in Sub-seasonal Predictability: *SUB SEASONAL TO SEASONAL PREDICTION: The Gap Between weather and Climate Foreasting*, A. W. Robertson and F. Vitart, eds., Elsevier Inc.,201-221.

[12] Fraedrich, K., H. Jansen, E. Kirk, U. Luksch, and F. Lunkeit, 2005: The Planet Simulator: Towards a user-friendly model, *Meteorologische Zeitschrift* **14(3)**, 299-304, doi:10.1127/0941-2948/2005/0043.

[13] Maier-Reimer, E., U. Mikolajewicz and K. Hasselmann, 1993: Mean circulation of the Hamburg LSG OGCM and ist sensitivity to the thermohaline surface forcing, J. Phys., Oceanogr., **23**, 731– 757, doi:10.1175/1520-0485(1993)023<0731:MCOTHL>2.0.CO;2.

[14] Chevallier, M. and D. Salas-Mélia, 2012: The Role of Sea Ice Thickness Distribution in the Arctic Sea Ice Potential Predictability: A Diagnostic Approach with a coupled GCM, *Journal of Climate*, **25(8)**, 3025-3038, doi:10.1175/JCLI-D-11-00209.1.

[15] EUMETSAT Ocean and Sea Ice Satellite Application Facility, 2024: Monthly Mean Northern Hemisphere Sea Ice Area from EUMETSAT OSISAF, v2p2, OSI-420, Norwegian Meteorological Institute, accessed 13 February 2025: ftp://osisaf.met.no/prod_test/ice/index/v2p2/nh/osisaf_nh_sia_monthly.nc.

[16] Kapsch, M.-L., N. Skific, R. G. Graversen, M. Tjernström, and J. A. Francis, 2019: Summers with low Arctic sea ice linked to persistence of spring atmospheric circulation patterns, Climate Dynamics, 52, 2497-2512, doi: 10.1007/s00382-018-4279-z.